

STATISTICAL DOWNSCALING FOR FUTURE EXTREME WAVE HEIGHTS IN THE NORTH SEA

BY ROSS TOWE*,¹, EMMA EASTOE*, JONATHAN TAWN*
AND PHILIP JONATHAN[†]

Lancaster University and Shell Research Limited, UK[†]*

For safe offshore operations, accurate knowledge of the extreme oceanographic conditions is required. We develop a multi-step statistical downscaling algorithm using data from a low resolution global climate model (GCM) and local-scale hindcast data to make predictions of the extreme wave climate in the next 50-year period at locations in the North Sea. The GCM is unable to produce wave data accurately so instead we use its 3-hourly wind speed and direction data. By exploiting the relationships between wind characteristics and wave heights, a downscaling approach is developed to relate the large and local-scale data sets, and hence future changes in wind characteristics can be translated into changes in extreme wave distributions. We assess the performance of the methods using within sample testing and apply the method to derive future design levels over the northern North Sea.

1. Introduction. An important issue for the oil industry is the optimal design of offshore structures. If the strength of the offshore structure is underestimated, damage may occur more often than hoped for, whereas if the strength is overestimated the structure will be unnecessarily expensive to build. To ensure adequate protection at minimum cost, the distribution of peak wave heights in extreme storms needs to be estimated as efficiently as possible. Traditionally, this distribution is then summarised by a single value, the T -year return level, corresponding to the level exceeded by a stationary process once every T years. Many offshore structures are designed to withstand 1000–10,000 year return values of significant wave height (H), where H is the mean of the highest third of waves in a short period of time (i.e., either a 10- or 20-minute period) and is typically sampled 3-hourly [Kinsman (2012)]. Standard extreme value models, fitted to historical data, can be used to derive such return level estimates under the assumption of stationarity [Coles (2001)]. Robinson (1995) and Jonathan and Ewans (2007) show how to adapt these methods to account for directionality in sea currents and H , respectively. The benefit of having directional return level information is that the structures can be designed to have differential strength from different sectors, which can lead to improved safety and cost savings.

Received October 2016; revised May 2017.

¹Supported by Shell Research Limited, UK.

Key words and phrases. Climate change, covariate modelling, environmental modelling, extreme value theory, sea waves, statistical downscaling.

When designing structures to last, say, 50 years forward, the probable influence of climate change makes the assumption of a stationary wave process too simplistic. The changing dynamics of the climate system [Solomon et al. (2007)] need to be accounted for in estimates of return levels of H for future years. There is no consensus on the exact effects of climate change [Lofsted (2014)]. Within the observational data record of H , typically 50 years, any climate change signal is hard to detect as it will be due to the combined effects of a number of physical processes, some of which may be observed, whilst others will be unobserved. Further, changes predicted by climate models for this period, are small relative to changes predicted in the coming 50 years [Easterling et al. (2000)], so that even if we could use a regression-type model fitted to the observed data to describe current change, this would not provide reliable future estimates of return levels as the covariates would also need to be predicted into the future.

In this paper, we focus on obtaining predictions of future H across a grid of locations in the northern North Sea, in order to estimate the kinds of return levels discussed above. To account for the effects of climate change, we use output from the HADGEM2 RCP 8.5 General Circulation Model (GCM), obtained from the Hadley Centre of the UK Met Office (UKMO). GCMs in general are run over a coarse grid, and for a range of future climate change scenarios, to derive potential future climates [Edwards (2010)]. HADGEM2 RCP 8.5 has the strongest climate change signal of all the UKMO's standard GCMs [Bellouin et al. (2011)], and so any changes in return levels found using it could be viewed as an upper bound on the potential change in design, with the bound derived over typical climate change scenarios. Output is available from 1960 to 2100.

Since GCMs have coarse grids, it is optimistic to assume their output will provide reliable future values for physical variables at a given location. For example, HADGEM2 has only six $120 \text{ km} \times 140 \text{ km}$ grid boxes covering the northern North Sea. Both wind and wave values vary dramatically within even one of the GCM cells due to land shadows. Instead, some kind of transformation is required. Downscaling, either dynamical or statistical, is widely used to achieve this [Maraun et al. (2015)]. Dynamical downscaling integrates GCMs with finer scale numerical models to produce regional climate models. This approach is computationally costly and passes biases in the GCM down to local inference. Statistical downscaling develops empirical relationships between data from the location of interest and the associated GCM variable and then uses changes in the distribution of the GCM data over time to infer changes in the distribution of the variable of interest at the required location. There are three types of statistical downscaling approaches; weather typing, weather generators and regression methods/transfer functions [Maraun et al. (2015)], with regression-based approaches including multiple linear regression, canonical correlation analysis, neural networks and kriging [Wilby et al. (2004)]. In recent years, hybrid methods such as Casas-Prat, Wang and Sierra (2014) have also been developed, which combine multiple regression analysis with a weather typing approach.

It is impossible to downscale H directly as very few GCMs contain H , and, if they do, the predictions are highly unreliable [Wilby et al. (2004)]. However, GCMs regularly produce wind fields and so we can downscale these and then link winds to waves. To do this, we use data for wind produced by an atmospheric model and waves from the fine scale regional model WAM [Reistad et al. (2011)]. Together, we have wind and wave data for 100 “local” $40\text{ km} \times 40\text{ km}$ grid boxes, covering the northern North Sea, for the period 1960–2009. The wave hindcast data have been calibrated with observational data and are widely regarded as being very reliable over this region [Reistad et al. (2011)].

As identified by Kinsman (2012), the integrated effect of wind speed over the distance of the location from the coast (termed the fetch) determines the height of the waves. Fetch can change rapidly with direction in the North Sea due to land shadow effects from Norway and the Shetland Isles, with the largest waves coming from the longest fetches associated with the Arctic and Atlantic Oceans and with more moderate waves driven by winds from the southern North Sea. Consequently, wind direction is critical in determining wave height. Further, the North Sea basin is wind-wave driven, with all of the extreme waves arising as a result of local extreme wind speeds; swell waves, generated by low wind speeds over long time periods external to the North Sea basin, are not a source of extreme wave heights here. Evidence to support this is in given in Towe (2015).

The graphical model in Figure 1 shows the relationships between wind and wave processes for our North Sea data set. The graph shows two types of nodes, the light grey square nodes represent GCM variables and all other nodes represent hindcast variables from the regional wave hindcast model. The relationships within the wave hindcast variables are observational links, represented in Figure 1 by solid black lines, whereas the relationship between the GCM and the wave hindcast are distributional links and are represented by the dashed black lines.

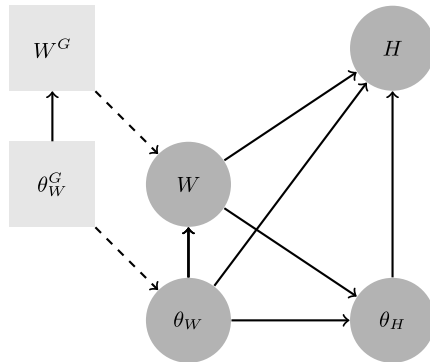


FIG. 1. Relationships between the variables wind direction (θ_W), wave direction (θ_H), wind speed (W) and how they relate to significant wave height (H). Variables with and without superscript (G) are from the GCM and wave hindcast data, respectively. Solid black lines represent observational links between the variables; dashed line are distributional links.

In order to produce estimates of the future distribution of H , we first model the relationships between the wave hindcast variables. Data from the GCM and wave hindcast for the “past” period are then used to derive links between the variables at the two spatial scales. Finally, the future values of the GCM outputs are used to derive the distribution of future H . The physical processes that link wind to waves are invariant to climate change so the past conditional relationship of H on the predictors (wind speed, W , with wind and wave directions, θ_W and θ_H , resp.) can be assumed to be preserved under climate change. When linking the wave hindcast and GCM, we use the nearest neighbour GCM grid cell to the wave hindcast grid location; exploratory analysis suggested there was no benefit from using additional GCM grid boxes.

Previous research on downscaling and climate change has restricted downscaling to variables directly outputted by the GCM, with the focus on predicting the mean rather than the extremes of a process. The closest approach to ours is [Caires, Swail and Wang \(2006\)](#) who use surface level pressure and proxies for wind speed as predictors in a regression analysis for H . Many studies, including [Caires, Swail and Wang \(2006\)](#), [Wang and Zhang \(2010\)](#) and [Vanem, Huseby and Natvig \(2012\)](#), have modelled extreme wave heights ignoring the critical effects of wind and wave direction, leading both to bias in return level estimates and a failure to provide vital design information [[Jonathan and Ewans \(2007\)](#)]. Inclusion of both wind speed and direction is vital as these variables have the strongest relationship with extreme waves heights and directions [[Towe et al. \(2013\)](#)].

Our statistical downscaling framework is likely to provide the most reliable estimates yet for determining future offshore design levels due to three substantial advances on existing methods. First, it models the joint distribution of $(H, W, \theta_H, \theta_W)$ at each location, both in the past and in the future, gaining insight over methods that only downscale H . Second, it uses state-of-the-art univariate and multivariate extreme value theory including more efficient threshold methods, and a broad class of asymptotically justified dependence models, which encompass methods used previously by [Bechler, Vrac and Bel \(2015\)](#) as a special sub-class. Finally, our approach uses a novel form of distributional downscaling that overcomes some major weaknesses with existing methods.

Our model currently has no spatial structure imposed on the joint distributions at different locations; over space the distributions of the variables will change relatively smoothly, following smooth changes in the empirical joint distributions. Using our current methods, it is not possible to generate spatial coherent joint events; see [Section 5](#) for further discussion. However, if interest is in the joint distributions of oceanographic variables at each location separately, our method is ideal as it is easily parallelisable.

The layout of the paper is as follows. [Section 2](#) outlines the core statistical methodology that we use under idealised assumptions. [Section 3](#) presents the inference for the components of the graphical model shown in [Figure 1](#), covering extensions of the methods of [Section 2](#) to handle covariates, assessment of fit and an algorithm for simulating future values. [Section 4](#) illustrates the downscaling al-

gorithm producing the estimated distribution of future H irrespective of, and conditionally on, wave direction. Two examples of prediction for a single site from the wave hindcast data set are shown: in Section 4.1, we predict the distribution for the last 10 years of observations as a validation exercise, then predictions are made for 2040–2049. The latter application is then implemented over a grid in the northern North Sea in Section 4.2. The 2040–2049 period was chosen as this is towards the end of the design lifetime of an offshore structure constructed today, so return levels in this period are critical for present day designs.

2. Background to modelling methodology.

2.1. *Modelling marginal distributions with focus on their tails.* Marginal models are needed for wind direction and speed, and for wave height and direction. In what follows, let Y denote a continuous random variable, with marginal distribution function K_Y . The model for K_Y needs to be applicable across many sites, so a simple choice is to use the kernel smoothed cumulative distribution function $\tilde{K}_Y(y)$ [Silverman (1986)]. This method is known to work poorly for the tails of the distribution, therefore, in the upper tail we replace the kernel estimate with a model motivated by univariate extreme value theory [Coles (2001)]. This is particularly critical for wind speeds and wave heights, since it is the upper extremes of these variables that are central to our model.

Consider the excess by Y of a high threshold u . Limit theory states that the only possible nondegenerate limit distribution for the appropriately scaled excesses, as u tends to the upper end point of K_Y , is the generalised Pareto distribution (GPD) [Davison and Smith (1990)]. Assuming that this limit distribution holds for a given threshold u , with $\mathbb{P}(Y > u)$ being small, motivates the model

$$(2.1) \quad \mathbb{P}(Y - u \geq y | Y > u) = \left(1 + \frac{\xi}{\sigma_u} y\right)_+^{-1/\xi} \quad \text{for } y > 0,$$

with scale parameter $\sigma_u > 0$ dependent on the threshold choice, shape parameter $\xi \in \mathbb{R}$ and $y_+ = \max\{y, 0\}$. The case $\xi = 0$ is interpreted as $\xi \rightarrow 0$. Diagnostics for the choice of u are discussed in detail by Coles (2001). The power of this result is that threshold excesses are restricted to a single parametric family, the GPD, regardless of the form of K_Y .

Combining the kernel smoothed distribution and GPD models gives

$$(2.2) \quad K_Y(y) = \begin{cases} \tilde{K}_Y(y) & \text{for } y \leq u, \\ 1 - \lambda_u [1 + \xi(y - u)/\sigma_u]_+^{-1/\xi} & \text{for } y > u, \end{cases}$$

where $\lambda_u = 1 - \tilde{K}_Y(u)$. We term this the $\text{GPD}(u, \lambda_u, \sigma_u, \xi)$ tail model. The T -year marginal return level y_T , found by solving $K_Y(y_T) = 1 - (mT)^{-1}$, is given by

$$(2.3) \quad y_T = u + \frac{\sigma_u}{\xi} [(Tm\lambda_u)^\xi - 1],$$

where m is the number of observations of the process in a year and $T > (m\lambda_u)^{-1}$.

We can incorporate covariates in the models for either, or both, the body and the tail, following the methods of [Davison and Smith (1990)]. Denote by C a vector of covariates associated with Y , then write

$$(2.4) \quad K_{Y|C}(y) = \begin{cases} \tilde{K}_{Y|C}(y) & \text{for } y \leq u_C, \\ 1 - \lambda(C)[1 + \xi(C)(y - u_C)/\sigma_u(C)]_+^{-1/\xi(C)} & \text{for } y > u_C, \end{cases}$$

where $\tilde{K}_{Y|C}(y)$ is a kernel smoothed conditional cumulative distribution of $Y|C$. The covariate-varying threshold u_C is taken to be the q th quantile of $Y|C$, which we obtain by solving $\tilde{K}_{Y|C}(u_C) = q$; giving $\lambda(C) = 1 - q$. Other authors have used quantile regression [Northrop and Jonathan (2011)] to determine u_C . Return levels can be obtained similar to the unconditional GPD tail model, except now care needs to be taken to distinguish between conditional and marginal return levels; for more details, see Eastoe and Tawn (2009).

In the above covariate model, it is usually assumed that the parameters $\sigma_u(C)$ and $\xi(C)$ change as a smooth function of the covariate(s), for example, through Fourier or spline representations [Jonathan, Ewans and Randell (2014)]. For one of our variables, this is not the case and we use the following special case of model (2.4), in which there is a single covariate C with covariate space $[c_1, c_2]$. This space can be partitioned into $j = 1, \dots, J$ subsets, $\Omega_j = [\psi_{j-1}, \psi_j)$, with $\psi_0 = c_1$ and $\psi_J = c_2$, where $\psi_{j-1} < \psi_j$. Given a threshold u_C as in model (2.4), the threshold exceedances in each subset are assumed to follow the GPD tail model with parameters $(u_C, \lambda(C), \sigma_{u,j}, \xi_j)$. The partitioning parameters $\psi_1, \dots, \psi_{J-1}$ can be specified in advance, or estimated as model parameters. We choose to do the latter since this enables the model to be fitted automatically, reduces user-subjectivity in the model fit and speeds up the modelling process when applied across multiple sites.

2.2. Transform methods. Transform methods are used to relate the large scale X (GCM) and local scale Y (wave hindcast) variables. Past data (X_P and Y_P) are available for both X and Y whereas future data (X_F) are available for X only. Our goal is to estimate the distribution of Y in the future (Y_F). Two fundamental assumptions are made. First, that for a given spatial scale and time period, each of the variables is identically distributed, but that this distribution may differ between spatial scales and time periods. Second, that the change in the distribution from Y_P to Y_F is a direct consequence of the change in distribution from X_P to X_F . Here, the standard transformation method for CDF downscaling is introduced, its weaknesses are identified and novel approaches are presented to overcome these deficiencies.

Michelangeli, Vrac and Loukos (2009) define the CDF-transform model for the distribution of Y_F as

$$(2.5) \quad K_{Y_F}(y) = K_{Y_P} \{ K_{X_P}^{-1} [K_{X_F}(y)] \},$$

where the distribution function K is indexed by the associated variable. The key part of this expression is $K_{X_P}^{-1}[K_{X_F}(\cdot)]$, which implies that changes in the distribution from Y_P to Y_F correspond to changes at a quantile scale in the distribution of X_P to X_F , where the latter changes can be attributed to climate change. Michelangeli, Vrac and Loukos (2009) estimate K_{Y_F} using kernel smoothed estimates for each term in the right-hand side of expression (2.5). For extreme event data, Kallache et al. (2011) model each distribution on the right-hand side of equation (2.5) using a GPD. They call this the xCDF-transform method. If different GPD parameters are used for Y_P , X_P and X_F , the distribution of the excesses $Y_F^* = Y_F - u | Y_F > u$, for $y > 0$, is

$$(2.6) \quad K_{Y_F^*}(y) = 1 - \left\{ 1 + \frac{\xi_{Y_P} \sigma_{X_P}}{\xi_{X_P} \sigma_{Y_P}} \left[\left(1 + \frac{\xi_{X_F}}{\sigma_{X_F}} y \right)_+^{\xi_{X_P}/\xi_{X_F}} - 1 \right]_+ \right\}_+^{-1/\xi_{Y_P}}$$

where here we drop the threshold indices from the scale parameters and indicate the associated variable through the indices of all parameters.

There are a number of limitations to this approach. First, the variables Y_P , X_P and X_F need to follow a GPD. Second, for effective performance of these approaches, each of the distributions has to have the same support and broadly similar variability. Third, and most fundamentally, the X and Y variables need to be measured in the same units of measurement, otherwise it does not make sense to evaluate, in equation (2.5), the probability $K_{X_F}(y)$, where y is on a completely different measurement scale to X .

None of these restrictions are guaranteed to hold. In general, we can only justify approximating the tails, and not the entire distribution, of each variable as GPD. Further, there is no reason to suppose that the X and Y variables will have the same support and measurement scales. For example, if X and Y represent wind speed and wave heights, respectively, then they are both on different scales and recorded in different units.

Kallache et al. (2011) attempt to overcome the second condition by restricting the support to be unbounded, that is, imposing that ξ_{X_P} , ξ_{X_F} and ξ_{Y_P} are all positive, and by *ad hoc* pre-processing of the variables through a location and scale transformation to make the observed ranges of the variables identical and the variables dimensionless. In what follows, we provide two extensions of the core method of Kallache et al. (2011) which seek to extend beyond the GPD assumption, formalise the pre-processing method and relax the assumption of unbounded support.

Both extensions use the following basic alteration to the xCDF-transform. Based on the premise that interest is in the whole distribution and not just the tails, we model the terms in the right-hand side of expression (2.5) using the GPD tail model (2.2). The thresholds for each variable may be different and must be selected in advance. Throughout, we take the threshold exceedance rate to be constant over variables [Kyselý, Picek and Beranová (2010)], that is, $\lambda_{Y_P} = \lambda_{X_P} = \lambda_{X_F} = \lambda$. The resulting downscaled distribution function for Y_F has tail behaviour,

for $y > u_{Y_F}$,

$$\begin{aligned}
 (2.7) \quad K_{Y_F}(y) = & 1 - \lambda \left[1 + \frac{\xi_{Y_P}}{\sigma_{Y_P}} (u_{X_P} - u_{Y_P}) \right. \\
 & \left. + \frac{\sigma_{X_P}}{\xi_{X_P}} \left\{ \left[1 + \xi_{X_F} \left(\frac{y - u_{X_F}}{\sigma_{X_F}} \right) \right]_+^{\frac{\xi_{X_P}}{\xi_{X_F}}} - 1 \right\} \right]^{-1/\xi_{Y_P}}.
 \end{aligned}$$

If, in addition, $\xi_{X_P} = \xi_{X_F}$, then Y_F has a GPD($u_{Y_F}, \lambda, \sigma_{Y_F}, \xi_{Y_P}$) tail model where

$$u_{Y_F} = u_{X_F} + \frac{\sigma_{X_F}}{\sigma_{X_P}} (u_{Y_P} - u_{X_P}) \quad \text{and} \quad \sigma_{Y_F} = \frac{\sigma_{Y_P} \sigma_{X_F}}{\sigma_{Y_P}}.$$

Model (2.7) can easily be extended to allow the distributions for Y_P , X_P and X_F to be modelled conditionally on covariates, by use of the conditional tail model (2.4). We refer to this as the cCDF-transform, where ‘‘c’’ stands for conditional (on covariates). We illustrate this approach in Section 3.3.

Like the original xCDF-transform, distribution (2.7) can only be applied when all the component distributions have the same upper endpoint, which requires the three shape parameters to have the same sign and imposes additional constraints when they are all negative. To resolve this issue, our first extension (E1), applies a model-based scaling factor to ensure that the distributions have a common upper end-point, predict Y_F on this new scale, and then transform back onto the original scale, thus formalising the idea of Kallache et al. (2011). Further details are given in the Appendix, with an application to wind speeds in Section 3.3.

Unfortunately, extension E1 is not ideal as it does not extend to cases where the variables have a mixture of finite and infinite upper endpoints, nor to cases where scaling using tail quantiles gives different variability to the scaled distributions. Instead, we propose our second extension (E2) in which we derive a new transformation approach which has a very different assumption. Specifically, we assume that there exists a single strictly increasing monotonic function A such that the distributions of $A(X_P)$ and $A(X_F)$ are identical to those of Y_P and Y_F , respectively. This is a strong assumption, and we will see later that the identification of A is sometimes nontrivial, resulting in the need then to fall back on extension E1 above.

Suppose, for now, that A can be identified, then this says that the change in marginal distribution from Y_P to Y_F is given by a deterministic effect of the change in marginal distribution from X_P to X_F . Therefore, for all y ,

$$(2.8) \quad K_{Y_F}(y) = \Pr(A(X_F) < y) = K_{X_F}(A^{-1}(y)),$$

with the support of Y_F being $D_{Y_F} = \{y \in \mathbb{R} : 0 < K_{Y_F}(y) < 1\}$ and the distribution K_{X_F} estimated using the GPD tail model. Notice that the assumption also implies that for all y and all $p \in [0, 1]$

$$K_{Y_P}(y) = K_{X_P}(A^{-1}(y)) \quad \text{and} \quad K_{Y_P}^{-1}(p) = A(K_{X_P}^{-1}(p))$$

so that

$$A^{-1}(y) = K_{X_P}^{-1}(K_{Y_P}(y)) \quad \text{for } y \in D_{Y_P}$$

and

$$A(x) = K_{Y_P}^{-1}(K_{X_P}(x)) \quad \text{for } x \in D_{X_P},$$

where D_{X_P} and D_{Y_P} are the support of X_P and Y_P , respectively. The function A maps any quantile of X_P to the same quantile for Y_P , and thus the functional form for A can be obtained by looking at a quantile-quantile plot of X_P and Y_P .

As set out above, A is defined only over $x \in D_{X_P}$ (or equivalently A^{-1} for $y \in D_{Y_P}$), whereas we require it over $x \in D_{X_F}$ (or equivalently A^{-1} for $y \in D_{Y_F}$). If the support of X_F is a subset of the support of X_P , that is, $D_{X_F} \subseteq D_{X_P}$ then

$$(2.9) \quad K_{Y_F}(y) = K_{X_F}(A^{-1}(y)) = K_{X_F}(K_{X_P}^{-1}(K_{Y_P}(y))),$$

and A can be estimated empirically using a quantile-quantile plot (possibly smoothed) of Y_P against X_P . Note that transformation (2.9) is very similar in structure to transformation (2.6), though critically it has the distributions in a different order so that now we have the natural property that we only ever evaluate the X (Y) distribution function with values taken on their respective measurement scale.

It is more likely that $D_{X_F} \not\subseteq D_{X_P}$, that is, the support of X_F is not a subset of the support of X_P . For example the distribution of X_F may have shifted compared to the distribution of X_P due to climate change. Consequently, the estimate of A identified on the domain $x \in D_{X_P}$ must then be extended into the domain $D_X = D_{X_P} \cup D_{X_F}$. There is no way theoretically to obtain a general functional form for A . Instead, an appropriate form, for example, linear, quadratic or exponential, may be found by examination of the quantile-quantile plot of X_P and Y_P for large X_P .

In practice, identification of a simple functional form for A may prove impossible, in particular if the distributions of X and Y vary in a nontrivial way with covariates. An instance when A is too complex to model occurs with wind speed (see Section 3.3). In this case, we suggest using instead extension E1. An application of extension E2 including the selection of an appropriate functional form for A , is shown for wave heights in Section 3.5.

Whichever method we use for the transformation, it is straightforward to simulate values of Y_F from these transformation models using the probability integral transform method. Simulated values for X_P and Y_P follow by quantile matching; if Y_F is simulated as the $p\%$ quantile from $K_{Y_F}(y)$, then concomitant values of the other variables are simulated as $p\%$ quantiles of their respective distributions.

2.3. *Conditional model for multivariate extreme values.* The downscaled W is used to predict H via a model for the bivariate extremal dependence behaviour of W and H . Consequently, we need to model the joint distribution of a bivariate random variable, which we denote by (Y_1, Y_2) , when at least one component of this variable is large. The methods presented here for the bivariate case were initially presented in the general multivariate case by [Heffernan and Tawn \(2004\)](#) but have novel elements due to downscaling.

The joint distribution of (Y_1, Y_2) is determined by its marginal distributions and its copula [[Nelsen \(2006\)](#)] and to estimate the extremal dependence structure of the random variables (Y_1, Y_2) , it is standard to estimate the marginal distributions and transform the variables onto a common scale [[de Haan and Ferreira \(2010\)](#)]. Marginal models K_1 and K_2 are given by the GPD tail model (2.2). For reasons explained by [Keef, Papastathopoulos and Tawn \(2013\)](#), we then transform to Laplace margins:

$$(2.10) \quad S_i = T(Y_i) = \begin{cases} \log\{2K_i(Y_i)\}, & Y_i < K_i^{-1}(0.5), \\ -\log\{2[1 - K_i(Y_i)]\}, & Y_i \geq K_i^{-1}(0.5) \end{cases}$$

for $i = 1, 2$. Consequently, S_i has exact exponential decay in both tails.

Now consider the extremal behaviour of the joint tail of (S_1, S_2) . There are infinitely many possible copula models but, as in the univariate case, asymptotic theory can be applied to look for a parsimonious family of possibilities when we restrict ourselves to the extremes only. Multivariate extreme value theory [[de Haan and Ferreira \(2010\)](#), [Ledford and Tawn \(1996\)](#)] has identified fundamentally different behaviour in the properties of the joint extremes depending on the value of

$$(2.11) \quad \chi = \lim_{v \rightarrow \infty} \mathbb{P}(S_2 > v | S_1 > v),$$

with $\chi > 0$ and $\chi = 0$ termed asymptotic dependence and asymptotic independence, respectively. Since most multivariate extreme value models [[Coles and Tawn \(1994\)](#), [de Haan and de Ronde \(1998\)](#)] and all max-stable processes [[Bechler, Vrac and Bel \(2015\)](#), [Davison, Padoan and Ribatet \(2012\)](#)] can model asymptotic dependence only, we shall use the conditional extreme value model of [Heffernan and Tawn \(2004\)](#), which includes both asymptotic dependence and asymptotic independence.

[Heffernan and Tawn \(2004\)](#) and [Keef, Papastathopoulos and Tawn \(2013\)](#) found that for a wide range of copulas there exist parameters $-1 \leq \alpha \leq 1$ and $-\infty < \beta < 1$ and a nondegenerate distribution function $Q(z)$ such that for $w > 0$ and $z \in \mathbb{R}$,

$$(2.12) \quad \lim_{v \rightarrow \infty} \mathbb{P}\left(\frac{S_2 - \alpha S_1}{(S_1)^\beta} \leq z, S_1 - v > w \mid S_1 > v\right) = \exp\{-w\}Q(z).$$

In addition some joint conditions on α, β and Q are required [[Keef, Papastathopoulos and Tawn \(2013\)](#)]. [Heffernan and Resnick \(2007\)](#) found that (2.12) holds

under general conditions if the affine transformation of S_2 used suitable regularly varying functions. For statistical purposes, the representation in [Heffernan and Tawn \(2004\)](#) offers adequate flexibility and parsimony. If $\alpha = 1, \beta = 0$ the variables are asymptotically dependent and grow at the same rate. If $0 < \alpha < 1$ ($-1 < \alpha < 0$), the variables are positively (negatively) asymptotically independent, with the largest S_2 being unlikely to occur with the largest S_1 . Further, if S_1 and S_2 are interchanged, the formulation holds but with potentially different parameter values and limit distribution Q ; for discussion of the constraints to ensure self-consistency of these two conditional models, see [Liu and Tawn \(2014\)](#).

There are three features to note about limit (2.12): the first term arises from S_1 following a Laplace distribution; there is no closed-form parametric model for Q , so we estimate it nonparametrically under the assumption that its first two moments exist; and, given that $S_1 > v$, in the limit as $v \rightarrow \infty$, the normalised S_1 and S_2 are independent.

For statistical modelling, we assume that the limiting result (2.12) holds exactly above a sufficiently high dependence threshold v . If this assumption is valid, it follows that, given $S_1 > v$, the variable

$$(2.13) \quad Z = \frac{S_2 - \alpha S_1}{S_1^\beta},$$

has distribution Q with finite mean μ and variance ψ^2 , and is independent of S_1 . This results in the regression model

$$(2.14) \quad S_2 = \alpha S_1 + S_1^\beta Z \quad \text{for } S_1 > v, \text{ where } -1 \leq \alpha \leq 1, -\infty < \beta < 1,$$

where $\mathbb{E}[S_2|S_1 = s] = \alpha s + s^\beta \mu$ and $\text{Var}[S_2|S_1 = s] = (s^\beta \psi)^2$, for $s > v$. Estimates of α and β can be obtained using either moment estimation or regression, under the working assumption that Z follows a Gaussian distribution [see [Heffernan and Tawn \(2004\)](#)]. Once estimates of α and β are determined, Q is estimated using the kernel smoothed distribution function of the Z values (2.13). Whilst the Gaussian assumption can be relaxed by using Bayesian nonparametric methods [[Lugrin, Davison and Tawn \(2016\)](#)], in practice estimates are not greatly affected.

In the context of downscaling, we use the bivariate conditional extremes model for (X_P, Y_P) to simulate from the distribution of $Y_F|X_F$. The following simulation algorithm requires the assumption that the copulae for (X_P, Y_P) and (X_F, Y_F) are identical, but that the marginal distributions of the variables change. First, estimate the marginal and dependence parameters of the conditional multivariate extremes model using observations of (X_P, Y_P) . Next, estimate the marginal distribution K_{X_F} of X_F using previously downscaled values for this variable, and use this distribution to transform to Laplace margins S_{X_F} as in equation (2.10). Conditional on S_{X_F} , draw S_{Y_F} from the fitted dependence model (2.14). Finally, transform S_{Y_F} to the original margins, using distribution (2.8), with A identified

from a quantile-quantile plot of X_P and Y_P . Inverting this distribution function gives $Y_F = A(K_{X_F}^{-1}(L(S_2)))$, where L is the distribution function of a Laplace random variable. A discussion on modelling A is found in Section 3.5. Note that we cannot back transform K_{Y_P} directly since the support of X_P and X_F (or Y_P and Y_F) may differ.

3. Inference for components of the graphical model.

3.1. *Overview and notation.* Throughout the rest of the paper, we use the notation set out in Figure 1 and use superscripts as follows: G for GCM, P for past and F for future. The following models for the components of the graphical model in Figure 1 are presented:

1. Wind direction θ_W^F (clockwise from North, degrees) from which the wind propagates: distribution downscaled using the distributions $[\theta_W^P]$, $[\theta_W^{G,P}]$, and $[\theta_W^{G,F}]$ (Section 3.2).

2. Wind speed W^F (metres/sec): modelled distribution is $[W^F|\theta_W^F]$. Distribution downscaled using the distributions $[W_S^P|\theta_W^P]$, $[W_S^{G,P}|\theta_W^{G,P}]$, and $[W_S^{G,F}|\theta_W^{G,F}]$ (Section 3.3).

3. Wave direction θ_H^F (clockwise from North, degrees) from which the storm propagates: modelled distribution is $[\theta_H^F|\theta_W^F, W^F]$. Distribution determined by a directional regression model $[\theta_H^P|\theta_W^P, W^P]$ (Section 3.4).

4. Significant wave height H^F (metres): modelled distribution is $[H^F|W^F, \theta_H^F]$ using a bivariate conditional extreme values model for the distribution of $[H^F, W^F|\theta_H^F]$ derived from $[H^P, W^P|\theta_H^P]$ under the assumption that they have the same copulae (Section 3.5).

This section focuses on fitting the complete model for a single cell (location) in the wave hindcast data; this is then rolled out to all sites in Section 4.2. For each component, model fit at the single location is assessed using a variety of diagnostics, including fitting the models using the first forty years of past data (1960–1999), with the remaining ten years (2000–2009) held back and treated as the future for the purposes of model validation. This data split is also used to perform a validation exercise on the entire model (see Section 4.1).

To simplify modelling, it is helpful to assume independent and identically distributed (IID) realisations from the joint distributions of the variables in the GCM and wave hindcast data sets. To make these assumptions realistic, we model storm peak data only. In wave analysis, independent storm peaks are typically determined from the time series of H using a declustering algorithm [Jonathan and Ewans (2007), Smith and Weissman (1994)], which also minimises the effect of seasonality; in the North Sea extreme waves tend to occur in the winter only. Since H is unavailable in the GCM data, we instead select storms based on W . This

ensures consistency of declustering across the GCM and wave hindcast data sets. For each storm identified, we select the largest marginal value of W and concurrent values of the other variables of interest. Declustering is carried out separately for the two spatial scales. Because of the multi-level nature of the model, we use a nonparametric block bootstrap to derive confidence intervals. Blocks of 7 days are used, as this is longer than our declustering interval. To replicate the seasonal patterns, blocks selected for a given time period in the year are only drawn from the corresponding time periods in the data.

3.2. *Wind direction.* The CDF-transform method (Section 2.2) is used to downscale the distribution of θ_W^F . As the prevailing wind over the North Sea is from the south-west, the distribution of θ_W has most mass in the interval (180, 270), with a secondary mode from the north (310, 50). These modes hold regardless of spatial-scale (GCM/hindcast) and time period (P/F). To preserve these features, and to ensure continuity of the density function over 0 and 360 degrees, we considered both cyclic (von Mises) [von Mises (1964)] and noncyclic (Gaussian) kernels. For the Gaussian kernel, the data were repeated with shifts of 360 and the resulting density normalised over (0, 360). Both approaches gave similar results.

Figure 2(a) compares the empirical distributions of θ_W^P , $\theta_W^{G,P}$ and $\theta_W^{G,F}$ across the past (1960–1999) and validation (2000–2009) periods. Since we are not predicting far into the future, the distribution of the GCM variable changes little across the two time periods. However, there is a clear difference between the distributions at the local and global scales. Figure 2(b) shows the downscaled distribution for

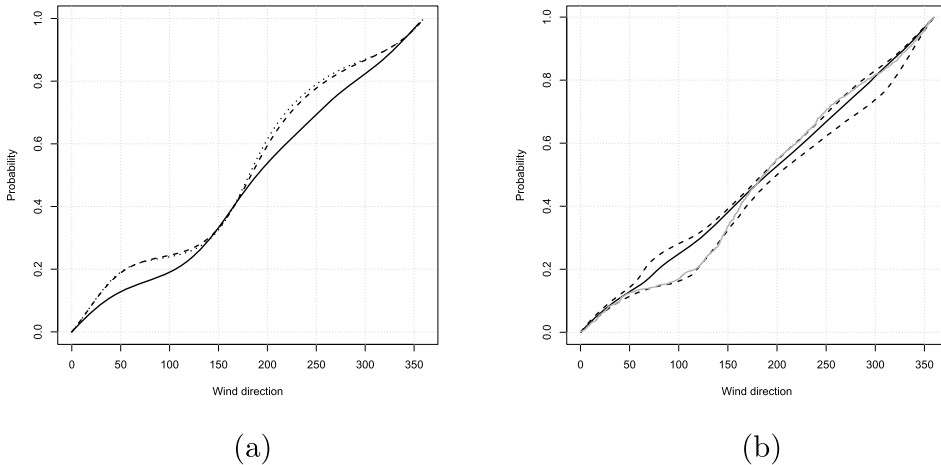


FIG. 2. Comparisons of (a) the empirical distributions of wind direction for θ_W^P (black), $\theta_W^{G,P}$ (dashed grey) and $\theta_W^{G,F}$ (dotted light grey); (b) the downscaled distribution for θ_W^F (black line) and 95% confidence intervals (dashed black lines) with the empirical distribution of θ_W^F (grey line). In both cases, past (P) is 1960–1999 and future (F) is 2000–2009.

θ_W^F in the validation period, compared with the empirical distribution of observed θ_W for the same period. The downscaled distribution appears to be almost uniform, whereas the empirical distribution appears bi-modal. However, the empirical distribution does lie within the pointwise 95% confidence intervals of the downscaled distribution.

3.3. *Wind speed.* The cCDF-transform methods (Section 2.2) are adopted to downscale wind speed given wind direction. Through equation (2.6), we combine the three conditional distributions, $[W_S^P | \theta_W^P]$, $[W_S^{G,P} | \theta_W^{G,P}]$, and $[W_S^{G,F} | \theta_W^{G,F}]$ to give the downscaled conditional distribution for $W^F | \theta_W^F$ as

$$(3.1) \quad K_{W^F | \theta_W^F}(w) = K_{W^P | \theta_W^P} \{ K_{W^{G,P} | \theta_W^{G,P}}^{-1} [K_{W^{G,F} | \theta_W^{G,F}}(w)] \}.$$

Application of extension E2 of the cCDF-transform was found to be difficult in this case, since inclusion of wind direction as a covariate in the component distributions implies that the function A should also vary (smoothly) over wind direction. An exploratory investigation of the quantile-quantile plots of $(W^P, W^{G,P})$ for a number of directional sectors suggested no consistent functional form for A ; consequently we use extension E1 instead justified further by all of the component distributions having bounded support. Simulation from this distribution is by application of the probability integral transform, conditional on the values of $\theta_W^P, \theta_W^{G,P}, \theta_W^{G,F}$ obtained from the simulations in Section 3.2.

To model each of the conditional distributions on the right-hand side of distribution (3.1), we use the methods discussed in Section 2.1: a conditional kernel smoothed distribution below a pre-specified covariate dependent threshold and a covariate dependent GPD tail model (2.4) above this threshold. The former is given by

$$(3.2) \quad \tilde{K}_{W | \theta_W}(y) = \frac{\sum_{i=1}^n \Phi\left(\frac{y - W_i}{h_W}\right) \phi\left(\frac{\theta_W - \theta_{W,i}}{h_{\theta_W}}\right)}{\sum_{i=1}^n \phi\left(\frac{\theta_W - \theta_{W,i}}{h_{\theta_W}}\right)},$$

where W_1, \dots, W_n and $\theta_{W,1}, \dots, \theta_{W,n}$ are the respective joint samples of wind speeds and corresponding wind direction, h_W (h_{θ_W}) is the bandwidth for wind speed (direction) and Φ (ϕ) is the distribution (density) function of the standard Normal distribution. Here, as in Section 3.2, the data were wrapped to ensure the distribution functions $\tilde{K}_{W|0}$ and $\tilde{K}_{W|360}$ are identical. Further, it was found that the conditional kernel model fitted poorly to the very lowest values of W , most likely due to an edge effect. To resolve this, an unconditional kernel distribution was fitted to these points. Above the threshold, no evidence was found for either the scale or shape parameters of the GPD to vary with wind direction, and consequently the downscaled distribution simplifies to equation (2.7). There was evidence to retain separate shape parameters for $W^{G,P}$ and $W^{G,F}$, that is, $\xi_{W^{G,P}} \neq \xi_{W^{G,F}}$.

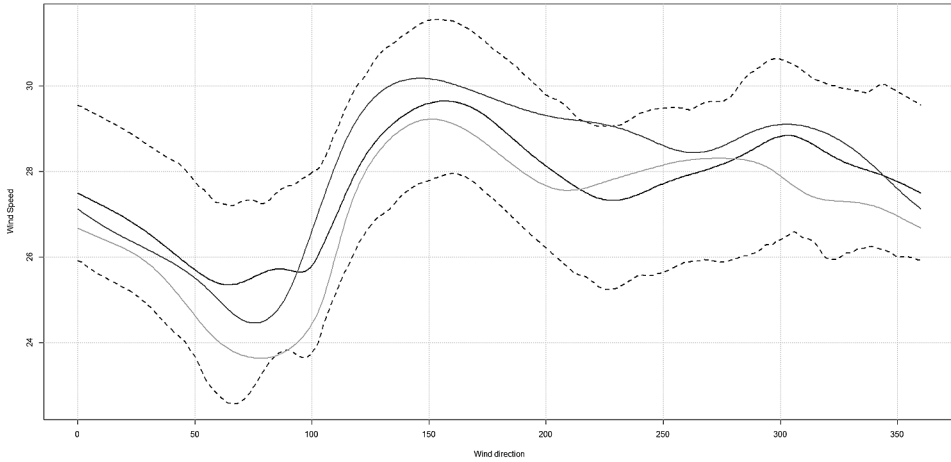


FIG. 3. Estimated 1 in 100 storm peak return values for wind speed W (ms^{-1}) conditional on wind direction θ_W (degrees): downscaling estimate (black line), with quantile regression based estimates obtained from past (1960–1999, light grey) and future (2000–2009, dark grey) wave hindcast data. Dashed black lines correspond to the pointwise 95% bootstrapped confidence intervals for the downscaled estimate.

Figure 3 shows the conditional 1 in 100 storm peak return value for wind speed, conditional on wind direction, as estimated from the above model. To interpret these return values, consider 100 arbitrary storms. These values show the direction-specific wind speed that we would expect to be exceeded once in the given direction when looking over all 100 storms. Note that this is not the same as the 1 in 100 storm peak conditional return value, which would look at the wind speed that we would expect to be exceeded once for each direction conditional on observing 100 storms from *that particular* direction. To assess how consistent this estimate is with the observed data, plots of the equivalent return levels estimated from the past (1960–1999) and future (2000–2009) wave hindcast data are also shown. These estimates were obtained directly from the respective data sets using a quantile regression on the 99% quantile. It is clear that the downscaled estimate follows a similar pattern to the estimate from the future wave hindcast data and, although the two estimates do not match exactly, the estimate from the future data does lie fairly well within the pointwise 95% confidence interval for the downscaled estimate.

3.4. *Wave direction.* Wave direction (θ_H) is driven by both wind speed (W) and direction (θ_W). Whilst this physical process may be susceptible to climate change, for example, through changes to sea level in shallower waters which would alter water depth, and thus also change the way in which wind-driven waves are produced, such changes are subtle and location-specific; we therefore assume that the distributional forms of $[\theta_H^F | \theta_W^F, W^F]$ and $[\theta_H^P | \theta_W^P, W^P]$ are identical. To determine the form of this conditional distribution, consider the difference $\theta_H - \theta_W$, as

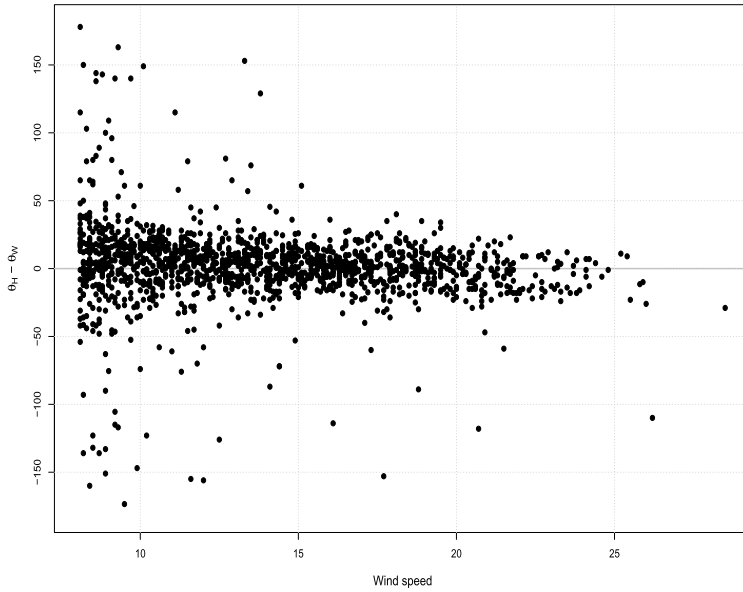


FIG. 4. The difference between wave θ_H and wind θ_W directions (degrees) plotted against wind speed W (ms^{-1}).

plotted against W , in Figure 4. For the very highest wind speeds, θ_H and θ_W are very similar as the local wave field is dominated by the behaviour of the wind. For lower wind speeds, average values of θ_H are still close to θ_W , however, there is greater variability of θ_H relative to θ_W since other factors, such as swell waves, have an increasing effect on the wave field [Bierbooms (2003)]. Consequently, we model $[\theta_H|\theta_W, W]$ as a mixture of von Mises distributions with mixture weight ω being a function of W ,

$$\begin{aligned}
 f_{\theta_H|\theta_W, W}(\theta_H) &= \omega(W) \frac{\exp\{\kappa_1 \cos[\theta_H - \theta_W - \mu_1]\}}{2\pi I_0[\kappa_1]} \\
 (3.3) \qquad \qquad \qquad &+ [1 - \omega(W)] \frac{\exp\{\kappa_2 \cos[\theta_H - \theta_W - \mu_2]\}}{2\pi I_0[\kappa_2]},
 \end{aligned}$$

where I_0 is the modified Bessel function of order 0; (μ_1, κ_1) and (μ_2, κ_2) are parameters to be estimated, and the mixture weight is modelled as a function of wind speed as follows:

$$(3.4) \qquad \qquad \qquad \omega(W) = \frac{\zeta \exp(\beta_0 + \beta_1 W)}{1 + \exp(\beta_0 + \beta_1 W)},$$

where $0 \leq \zeta \leq 1$. The mixture components can be thought of as models for wind directions associated with wind and swell waves, respectively. Since $\omega(W) \rightarrow \zeta \leq 1$ as wind speed gets large, including the scaling parameter ζ allows both wind and

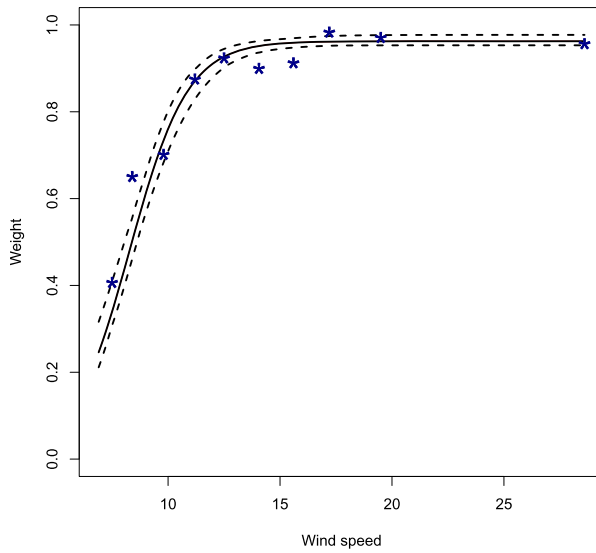


FIG. 5. Within block estimates of the mixture weight (points), with the estimate of $\omega(W)$ obtained from the full data sets given by the solid black line. Dashed lines show the pointwise 95% confidence interval for $\omega(W)$.

swell waves to occur at the highest wind speeds. For the strongest winds, if $\zeta < 1$, then both components will contribute to the overall mixture distribution, whereas if $\zeta = 1$, the mixture is determined by the “wind” component only.

To gain insight into this weight parameter, distribution (3.3) was first fitted to the entire data set assuming a constant weight $\omega(W) = \omega$. Next, the data set was divided into 10 equal-sized blocks, defined by the quantiles of wind speed. With the location and precision parameters for the two components fixed at the estimates obtained in the first step, and a constant mixture weight was estimated within each block, the resulting estimates of the weight parameter, shown in Figure 5, display a clear relationship with wind speed. The estimate of $\omega(W)$ obtained from the fit of the model described in equations (3.3) and (3.4) to the full data set, also shown in Figure 5, appears to follow the trend seen in the block estimates.

3.5. Significant wave height.

3.5.1. Overview. From Figure 1, significant wave height H is dependent on θ_W , θ_H and W . The conditional bivariate extremes approach of Section 2.3 is used to model the dependence structure between H and W , with dependence on wave and wind directions modelled through the conditional marginal distributions $H|\theta_H$ and $W|\theta_W$. Whilst it is possible to allow the conditional bivariate dependence model parameters to also vary with direction [Jonathan, Ewans and Randell (2014)], our data show no evidence to justify this additional model complexity.

Critical to our approach is that, unlike the marginal distributions, the copula for H and W is assumed not to change over time.

3.5.2. Marginal models. To fit the conditional bivariate extremes model, the marginal variables for (W^P, H^P) must first be transformed to a common marginal distribution using transform (2.10). For both margins, a threshold which varies with the conditioning variable (wind or wave direction) is used. Consequently, the distribution for $W^P | \theta_W^P$, denoted $K_{W^P | \theta_W^P}$, is the same as the one described in Section 3.3, that is, a GPD tail model with wind direction as a covariate. Furthermore, future values of W can be transformed using expression (3.1) for $K_{W^F | \theta_W^F}$.

The effect of wave direction on past H was found to be more complex than could be modelled by assuming a smooth change in the GPD model parameters with θ_H^P . This is largely due to the effect of the Norwegian sector, a region of directions from which storms are very rarely observed due to the limited fetch. Additionally, this sector varies over the grid of sites. Consequently, we apply the special case of the covariate GPD model discussed at the end of Section 2.1, with covariate space $[0, 360]^\circ$. We split this interval into three blocks $[0, \psi_1]$, $[\psi_1, \psi_2]$ and $(\psi_2, 360]$, with the interval $[\psi_1, \psi_2]$ denoting the Norwegian sector. A GPD model with parameters (σ_1, ξ_1) and a constant rate λ_1 is fitted to observed threshold exceedances of H^P for which θ_H^P is in either $[0, \psi_1)$ or $(\psi_2, 360]$. Similarly, a GPD model with parameters (σ_2, ξ_2) and constant rate λ_2 is fitted to observed threshold exceedances of H^P for which θ_H^P is in $[\psi_1, \psi_2]$. The partitioning parameters are estimated jointly with the GPD and rate parameters using a maximum likelihood function for all eight parameters. The resulting model is denoted $K_{H^P | \theta_H^P}$. Figure 6 shows a QQ plot which further demonstrates the goodness-of-fit of the Norwegian-sector model.

The distribution of $H^F | \theta_H^F$ is estimated using transformation method E2 and distribution function (2.8); the parameters of A were allowed to differ between the Norwegian and non-Norwegian sectors defined above. To choose the functional form of A , quantile-quantile plots of (H^P, W^P) for the two directional sectors were investigated; see Figure 7. In both cases, the relationship between the quantiles appears to be linear, at least for the highest quantiles. Thus we model A above a threshold v as linear, that is, $A(x) = a_{\theta_H} + b_{\theta_H}x$ for $x > v$. Consequently, the parameters a_{θ_H} and b_{θ_H} were estimated using only data from the quantile-quantile plots above the respective 80% quantiles of W . Figure 7 shows the fit appears to be good. This linear model is further supported by the known physical relationship between wind speed and wave heights in the North Sea [Kinsman (2012)]. Specifically, if all other factors were kept constant wave heights increase linearly with wind speed. In practice, the joint distribution of (H, W) is more complex due to factors such as the time period the wind blows and the direction of winds varying continually. The distribution of $H^F | \theta_H^F$ is estimated using transformation method E2 and distribution function (2.8); the parameters of A were allowed to differ between the Norwegian and non-Norwegian sectors defined above. To choose the

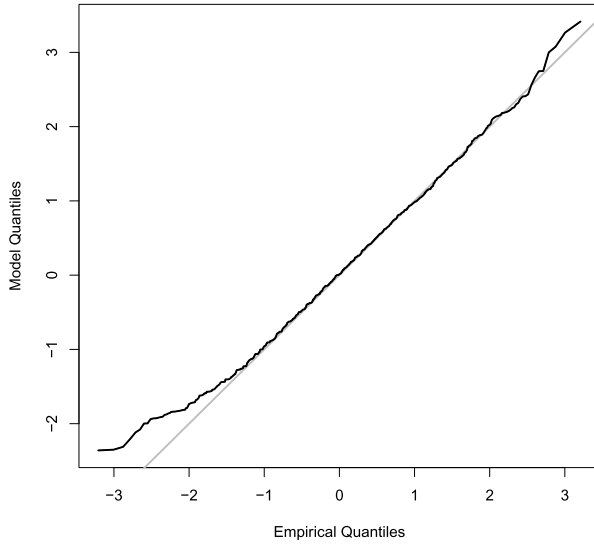


FIG. 6. *QQ plot to show the goodness of fit of the Norwegian-sector GPD model to $H|\theta_H$.*

functional form of A , quantile-quantile plots of (H^P, W^P) for the two directional sectors were investigated; see Figure 7. In both cases, the relationship between the quantiles appears to be linear, at least for the highest quantiles. Thus we model A above a threshold v as linear, that is, $A(x) = a_{\theta_H} + b_{\theta_H}x$ for $x > v$. Consequently, the parameters a_{θ_H} and b_{θ_H} were estimated using only data from the quantile-

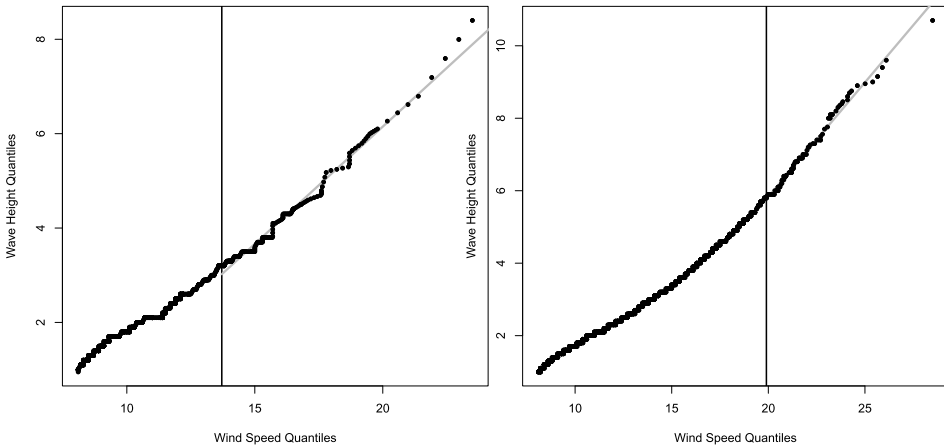


FIG. 7. *QQ plots of wind speed against significant wave height (black) for (a) the Norwegian sector and (b) data outside the Norwegian sector. In each case, above the 80% quantile of wind speed (black vertical line), the relationship between the quantiles is estimated by a linear model (grey).*

quantile plots above the respective 80% quantiles of W . Figure 7 shows the fit appears to be good. This linear model is further supported by the known physical relationship between wind speed and wave heights in the North Sea [Kinsman (2012)]. Specifically, if all other factors were kept constant wave heights increase linearly with wind speed. In practice, the joint distribution of (H, W) is more complex due to factors such as the time period the wind blows and the direction of winds varying continually.

3.5.3. Dependence modelling. Application of transform (2.10) using the above models, $K_{W^P|\theta_W^P}$ and $K_{H^P|\theta_H^P}$, results in Laplace variables (S_1, S_2) . The conditional bivariate extremes model is used to describe the distribution of $S_2|S_1 > v$ for large v . This is equivalent to $H^P|(W^P > T^{-1}(v), \theta_W^P, \theta_H^P)$, with T defined by expression (2.10) in which K_{Y_i} is replaced by $K_{W^P|\theta_W^P}$. Since we need to also capture the possibility that large H^P values may occur when W^P is not extreme, we need an additional model for $H^P|(W^P < T^{-1}(v), \theta_W^P, \theta_H^P)$, or equivalently for $S_2|S_1 < v$. A conditional kernel density is used for values of $s_1 < v$; although the resulting model for $S_2|S_1$ has a potential discontinuity at v , Towe (2015) found better fits were achieved without imposing continuity at v .

A dependence threshold corresponding to the 80% quantile of S_1 was chosen by using the diagnostic methods of Heffernan and Tawn (2004). Estimates (95% confidence intervals), of the key model parameters are $\hat{\alpha} = 0.78$ (0.4, 1) and $\hat{\beta} = 0.79$ (0.6, 1). Note that although the width of the confidence intervals of the two dependence parameters is large, the parameters themselves are negatively correlated and as a result a trade-off exists in their estimation. Furthermore, the resulting confidence intervals for the conditional mean of the process H^P are in fact narrower than one would expect given the variability of $(\hat{\alpha}, \hat{\beta})$; examples of this can be seen below. Thus there is a strong extremal dependence which includes asymptotic dependence inside the confidence intervals. For the less extreme values of S_1 , there is likewise a strong dependence with conditional quantiles of $S_2|S_1$ increasing almost at the same rate as quantiles of S_1 , clarifying that W^P is indeed a key driver of H^P across the full support of W^P .

We assess the fit of the model in three ways. Two graphical diagnostics are shown in Figure 8. First, the residuals, Z from the copula part of the fit of the conditional bivariate extremes model closely follow the assumed Gaussian distribution. Second, we compare a plot of observed H^P against W^P , to a simulation of N -storms from the model on common Laplace margins. The simulated data seem to reproduce the relationship seen in the observed data. The simulated data seem to reproduce the relationship seen in the observed data. Finally, empirical and model-based estimates of conditional expectations of $H^P|W^P > q$ show strong agreement across a range of values for q . Taking q to be the 95% quantile of W^P , the estimated conditional means of H^P are: model, 8.32, with a 95% confidence interval of (8.12, 8.52), and empirical, 8.23. Taking q to be the 99% quantile of W^P , the conditional means are: model, 9.16 (8.89, 9.43), and empirical, 8.98.

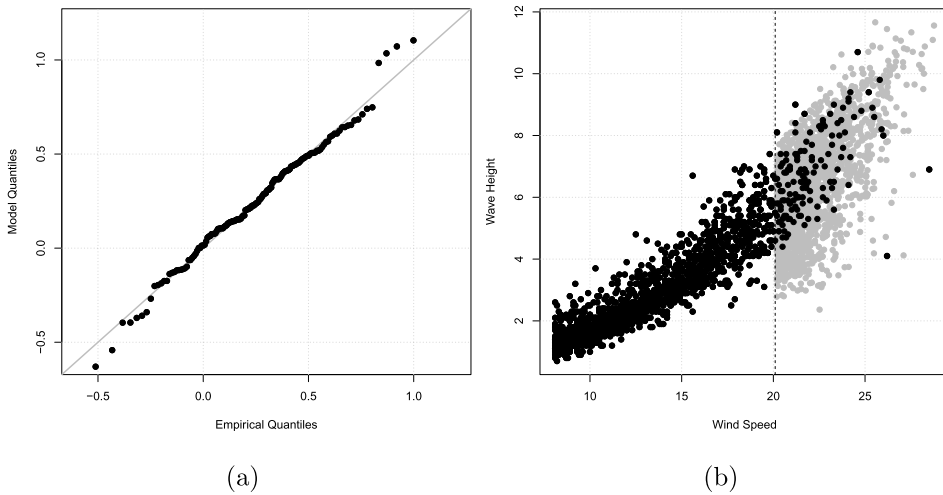


FIG. 8. (a) *Quantile-quantile plot of the residuals for the conditional bivariate extremes model compared to the $Normal(\mu, \psi)$ distribution.* (b) *Wave height against wind speed on Laplace margins: past data (black) with a data set simulated from the conditional bivariate extremes model (grey).*

4. Downscaled predictions.

4.1. *Prediction and model validation.* At a given location, the simplest way to obtain estimates of return levels, either marginal or conditional, for a given future period is by direct simulation from the model described in Section 3. A benefit of this approach is that it generates joint samples for $(W^F, \theta_W^F, \theta_H^F, H^F)$ and not simply the distribution of the downscaled variable, as in many existing downscaling methods. Return levels and joint characteristics can then be obtained empirically from the samples.

A natural way to predict a marginal m -year return level for a future decade is to simulate N years of storm peaks from the downscaling model for this decade, and take the appropriate largest order statistic as the estimate of the return level (i.e., to calculate the 50-year return level from 100 years of simulated storm peaks, the second largest order statistic is taken as the point estimate of the return level). However, this does not take into account simulation (Monte Carlo) uncertainty. To account for this, we used 100 replications of simulations of storm peaks each corresponding to 2000 years, with the median of the appropriate largest order statistic taken as the point estimate. To obtain a confidence interval for the return level, this process is repeated for all bootstrapped model fits. Further, investigations (not shown here) showed that the contribution due to simulation to the overall uncertainty in the return level estimates was much smaller than the contribution due to sampling. In terms of the uncertainty within the downscaling algorithm, the steps relating to W and H were found to cause the largest uncertainty.

To predict a conditional m -year return level, where conditioning is on wave direction, the same N -year simulated data set, as described above, can be used. Now though the simulations are binned into, say, 22.5° bins according to wave direction. The appropriate largest order statistic within each bin gives an estimate of the conditional m -year return level. Again, multiple simulations should be carried out, and the appropriate largest order statistic of the direction-wise estimates taken as the point estimate.

Return levels simulated using the above methods can be used in validating the model fitted to the past period 1960–1999, by a comparison of the downscaled return level estimates for the future data period 2000–2009 with the return level estimated from a tail model fitted directly to the wave hindcast data for the 2000–2009 period. To obtain marginal (conditional on wave direction) return levels directly from the 2000–2009 wave hindcast data the GPD tail model (2.2) and (2.4), respectively, are used.

Table 1 shows downscaled estimated marginal return levels for a single site for the decades 2000–2009 and 2040–2049. The return levels for 2040–2049 are larger than those for 2000–2009, for return periods of over 10 years, although all changes are within the 95% confidence limits. An issue with identifying statistically significant changes over this time period, due primarily to the W and H components. To improve the power of our methods for identifying change requires more efficient inference of these components. Spatial pooling for inference may help here, but this is not explored further.

We can also compare the downscaled conditional return levels for the same site and the same decades. For a return period of 10 years, Figure 9 shows both of these, along with the empirical conditional return levels for the period 2000–2009. All conditional return levels are given for sixteen nonoverlapping sectors, each of width 22.5° . The plot shows that the downscaling model is capturing well the general trend in H with θ_H . The 2000–2009 return levels for the Norwegian sector, which for this site was estimated as $(40^\circ, 120^\circ)$, are over-estimated compared to the empirical estimates; however, as θ_H is rarely in this sector this is not problematic. Downscaled return levels across the remaining sectors show no consistent

TABLE 1
*Single-site downscaled estimates of (and 95% confidence intervals)
for marginal return levels of significant wave height for the decades
2000–2009 and 2040–2049*

Return period (years)	2000–2009	2040–2049
10	13.41 (12.53, 15.57)	12.68 (10.34, 14.94)
50	15.10 (14.26, 18.24)	15.54 (12.15, 18.80)
100	15.70 (14.63, 19.11)	16.93 (12.87, 20.89)
200	16.28 (15.05, 19.97)	17.87 (13.58, 23.53)

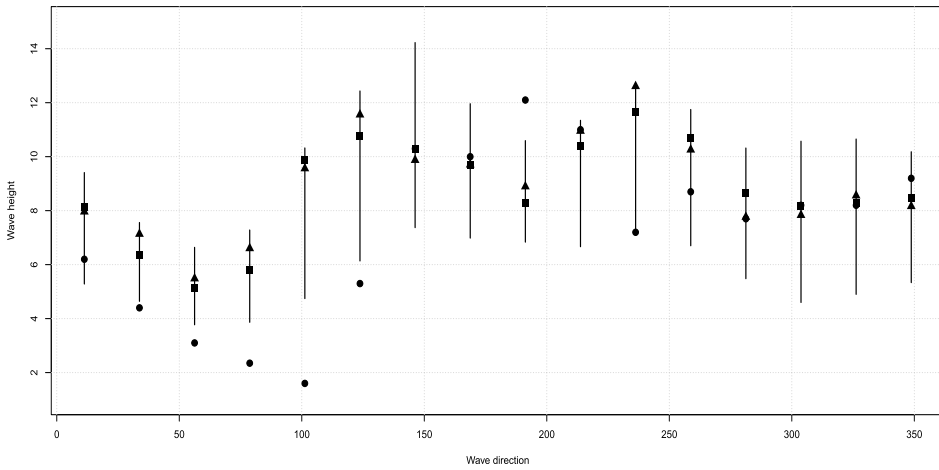


FIG. 9. Single-site conditional 10-year return levels of H for nonoverlapping 22.5° sectors of θ_H , starting with $[0, 22.5)^\circ$. Downscaled estimates are for the periods 2000–2009 (square) and 2040–2049 (triangle). Empirical estimates for 2000–2009 (circle) are also given. Vertical lines show bootstrapped confidence intervals on the downscaled 2000–2009 estimates. The estimate for each sector is plotted at its mid-point.

disagreement with their empirical equivalents. Further, there appears to be no obvious change in the return levels estimated for 2000–2009 and those estimated for 2040–2049. We can also compare the downscaled conditional return levels for the same site and the same decades. For a return period of 10 years, Figure 9 shows both of these, along with the empirical conditional return levels for the period 2000–2009. All conditional return levels are given for sixteen nonoverlapping sectors, each of width 22.5° . The plot shows that the downscaling model is capturing well the general trend in H with θ_H . The 2000–2009 return levels for the Norwegian sector, which for this site was estimated as $(40^\circ, 120^\circ)$, are over-estimated compared to the empirical estimates; however, as θ_H is rarely in this sector this is not problematic. Downscaled return levels across the remaining sectors show no consistent disagreement with their empirical equivalents. Further, there appears to be no obvious change in the return levels estimated for 2000–2009 and those estimated for 2040–2049.

4.2. *Spatial predictions for 2040–2049.* The downscaling algorithm is now implemented at all 100 locations on the 350 km by 350 km wave hindcast grid. For each location, the nearest GCM grid cell is chosen to provide the variables to be downscaled. Since wind behaviour differs markedly between land and sea, when the nearest GCM grid cell contains land the closest GCM grid cell that solely covers sea is chosen instead. Repeating a similar process to Section 4.1 a downscaled sample for 2040–2049 is used to derive estimates of the marginal and conditional return values for H^F site-by-site over the wave hindcast grid.

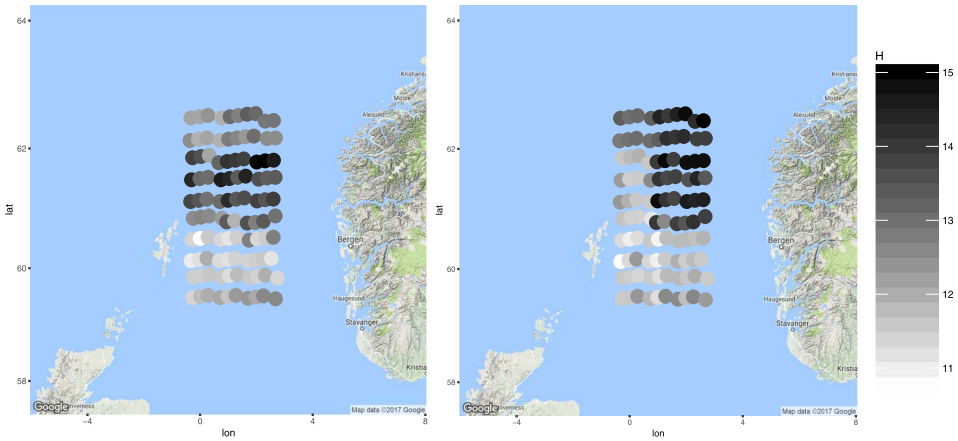


FIG. 10. Estimates of the marginal 10-year return levels for significant wave height at all locations in the North Sea study region: (left) 2000–2009 and (right) 2040–2049.

Figure 10 shows the 10-year marginal estimates for H^F for the decades 2000–2009 and 2040–2049. The spatial variability captures important known local features of the region: the lowest values are in the Shetland land shadow and the highest nearest to the Atlantic Ocean, though these estimates exhibit linear features linked to nearby sites having a common nearest GCM grid cell.

To illustrate the conditional return levels, we condition on wave direction θ_H^F being in one of the following directional sectors: Norwegian [20, 150), North Sea [150, 220) and Atlantic [220, 20). The conditional 10-year return levels for 2040–2049 for each site and each of the above sectors are plotted in Figure 11. From Figure 11, the land-shadow effect of the Shetlands is clear, since the highest return levels, conditional on a storm coming from the Atlantic sector, occur to the north of this group of islands. Conditioning on a storm coming from the southern North Sea, there is again a north-south trend in the return levels, with the less sheltered sites to the north generally having higher return values. In Figure 11, there is however an even clearer blocking pattern for each of the conditional directions than was apparent in the marginal estimates of Figure 10. Since this blocking is likely to be due to sites sharing a nearest GCM cell, a potential area for further research would involve determining the optimal weighting for the set of nearest GCM grid cells to a particular fine grid location.

5. Discussion and conclusions. This paper has developed a downscaling framework to predict extreme significant wave height. Our methods exploit recent advances in climate modelling by using global climate models to downscale wind speeds and directions jointly with wave height and direction. We have extended existing statistical transfer function downscaling techniques using a combination of generalised Pareto tails, covariate models, and two possible extensions to overcome their major limitations. We have also shown that multivariate extreme value

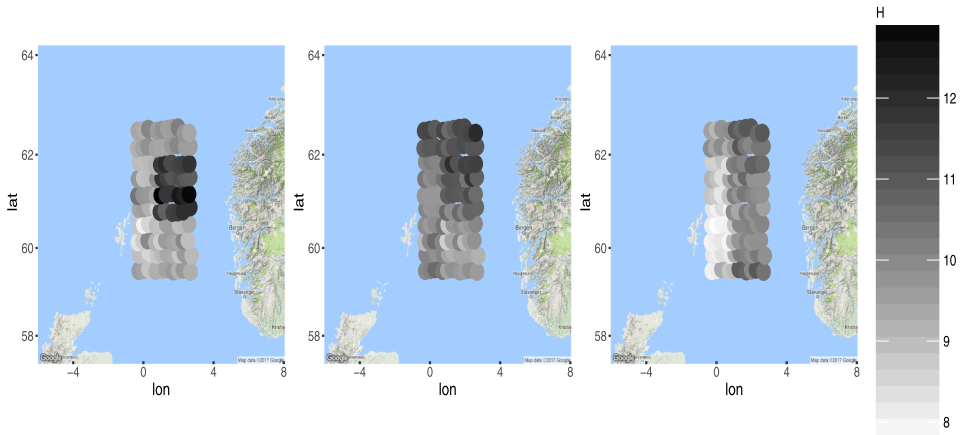


FIG. 11. Estimates of the conditional 10-year return levels for significant wave height in 2040–2049, where conditioning is on wave direction being in the sectors North Sea, Norwegian and Atlantic (left to right).

methods, in particular the conditional multivariate extremes model, can be used in statistical downscaling. Due to the use of local wind fields, the proposed implementation is only applicable to regions, such as the North Sea, where significant wave heights are dominated by wind waves rather than swell waves. For regions with swell dominated waves, which are generated outside the local area, global climate model grid cells for the area over which swell waves are generated would need to be used in the downscaling. Furthermore, wave period would need to be incorporated into the graphical model (Figure 1).

Our estimates of the future behaviour of the extreme wave climate of the North Sea show that the sizes of the largest waves, as well as the directions from which they arise, are changing within the lifetime of current offshore designs. For the return levels of 100 years or more, required for offshore design estimation, uncertainty somewhat obscures these changes. This uncertainty could be reduced by modifying the estimation of the distribution of $W^{G,F} | \theta_W^{G,F}$ in expression (3.1). In our approach, only data from the 10-year future period of the global climate model was used in this estimation, under the assumption that the distribution would not change over this period. However, since the climate is changing slowly and smoothly, a more efficient estimation of this distribution would be to fit this model over a longer time period than the 10 years of interest, and with time as an additional covariate. For example, it may be reasonable to fit this using data from 1960–2049. This provides additional data but avoids biasing estimates if longer-term climate changes from 2050 onwards are not well estimated. Such a model could then be applied by averaging this time changing distribution over the 2040–2049 period.

Our downscaling methodology is flexible enough to handle the varying marginal characteristics of the whole North Sea. However, the spatial nature of the processes

could be explicitly modelled both by imposing spatially smooth changes to the estimated component distributions of Section 3 and by estimating the joint extremes over sites through generating spatial events in the simulations. This should provide the added benefit of improving the marginal inferences as well by pooling spatial information. These issues are addressed in Davison, Padoan and Ribatet (2012) and Wadsworth and Tawn (2012) for models of processes which exhibit spatial asymptotic dependence and asymptotic independence, respectively. Our methodology provides a natural framework for incorporating these extensions and this remains an important area for future work.

APPENDIX: SCALING FACTOR FOR XCDF-TRANSFORM

When simulating under the xCDF-transform, it is assumed that the random variables X_P , X_F and Y_P share the same support. If the distributions of these variables have unequal, finite upper end-points, simulation of Y_F degenerates in the upper tail. To get around this, we simulate a re-scaled version of Y_F , by first re-scaling each of X_P , X_F and Y_P , before transforming back to the original scale.

In order to obtain the re-scalings required, first note that if $Y \sim \text{GPD}(\sigma, \xi)$, then, for any $\psi > 0$, the re-scaled variable $Y^* = Y/\psi$ also follows a GPD, with scale parameter σ/ψ and the same shape parameter ξ . Both Y and Y^* have finite end-points if and only if the shape parameter ξ is negative. For the original variable, Y , this end-point is $y^+ = -\sigma/\xi$, and for the re-scaled variable it is

$$(A.1) \quad m = -\frac{\sigma}{\psi\xi}.$$

Equivalently, to obtain a re-scaled variable Y^* with end-point m , we should re-scale by $\psi = -\sigma(m\xi)^{-1}$. Therefore, each of the following re-scaled variables shares a common end-point m :

$$(A.2) \quad \begin{aligned} X_P^* &= \frac{X_P}{\psi_{X_P}} = \frac{-m\xi_{X_P} X_P}{\sigma_{X_P}} \sim \text{GPD}(-m\xi_{X_P}, \xi_{X_P}), \\ X_F^* &= \frac{X_F}{\psi_{X_F}} = \frac{-m\xi_{X_F} X_F}{\sigma_{X_F}} \sim \text{GPD}(-m\xi_{X_F}, \xi_{X_F}), \\ Y_P^* &= \frac{Y_P}{\psi_{Y_P}} = \frac{-m\xi_{Y_P} Y_P}{\sigma_{Y_P}} \sim \text{GPD}(-m\xi_{Y_P}, \xi_{Y_P}). \end{aligned}$$

In practice, the parameters (σ_*, ξ_*) are obtained by modelling each variable on the original scale and the shared end-point m is specified by the user.

Simulation from the distribution of the re-scaled Y_F^* follows by direct application of the xCDF-transform to the GPD tail models for the re-scaled variables given in equation (A.2). To transform the predicted Y_F^* back to the original scale, $Y_F = \psi_{Y_F} Y_F^*$, requires the scaling factor $\psi_{Y_F} = -\sigma_{Y_F}(m\xi_{Y_F})^{-1}$; however, this is

unknown since there is no data which can be used to estimate $(\sigma_{Y_F}, \xi_{Y_F})$. We propose that ψ_{Y_F} be chosen so that the ratio between the end-points of Y_F and Y_P is the same as the ratio of the end-points of X_F and X_P , that is,

$$(A.3) \quad y_F^+ = y_P^+ \frac{x_F^+}{x_P^+}.$$

By re-arranging equation (A.1), it is clear that each variable has been scaled so that $m\psi$ is equal to the end-point of the original data. Therefore, equation (A.3) is equivalent to

$$\psi_{Y_F} = \psi_{Y_P} \frac{\psi_{X_F}}{\psi_{X_P}}$$

that is, the scaling factor for Y_F is selected so that the ratio between ψ_{Y_F} and ψ_{Y_P} is the same as the ratio between ψ_{X_F} and ψ_{X_P} . This scaling factor can then be applied to obtain $Y_F = \psi_F Y_F^*$.

Acknowledgements. Ross Towe would like to thank Nicolas Fournier for instigating this project. The GCM data was kindly provided by Simon Brown of the Met Office and we would like to thank David Randell of Shell Global Solutions for helpful discussions and the referees for suggestions that have improved our presentation.

REFERENCES

- BECHLER, A., VRAC, M. and BEL, L. (2015). A spatial hybrid approach for downscaling of extreme precipitation fields. *J. Geophys. Res., Atmos.* **120** 4534–4550.
- BELLOUIN, N., COLLINS, W., CULVERWELL, I., HALLORAN, P., HARDIMAN, S., HINTON, T., JONES, C., McDONALD, R., McLAREN, A., O'CONNOR, F. et al. (2011). The Hadgem2 family of Met Office unified model climate configurations. *Geosci. Model Dev.* **4** 723–757.
- BIERBOOMS, W. (2003). Wind and wave conditions. DOWEC (Dutch Offshore Wind Energy Converter Project) 47.
- CAIRES, S., SWAIL, V. and WANG, X. (2006). Projection and analysis of extreme wave climate. *Climate* **19** 5581–5605.
- CASAS-PRAT, M., WANG, X. and SIERRA, J. (2014). A physical-based statistical method for modeling ocean wave heights. *Ocean Model.* **73** 59–75.
- COLES, S. (2001). *An Introduction to Statistical Modeling of Extreme Values*. Springer, London. [MR1932132](#)
- COLES, S. and TAWN, J. (1994). Statistical methods for multivariate extremes: An application to structural design (with discussion). *J. R. Stat. Soc. Ser. C. Appl. Stat.* **43** 1–48.
- DAVISON, A. C., PADOAN, S. A. and RIBATET, M. (2012). Statistical modeling of spatial extremes. *Statist. Sci.* **27** 161–186. [MR2963980](#)
- DAVISON, A. C. and SMITH, R. L. (1990). Models for exceedances over high thresholds. *J. Roy. Statist. Soc. Ser. B* **52** 393–442. [MR1086795](#)
- DE HAAN, L. and DE RONDE, J. (1998). Sea and wind: Multivariate extremes at work. *Extremes* **1** 7–45. [MR1652944](#)
- DE HAAN, L. and FERREIRA, A. (2010). *Extreme Value Theory: An Introduction*. Springer, New York. [MR2234156](#)

- EASTERLING, D., MEEHL, G., PARMESAN, C., CHANGNON, S., KARL, T. and MEARNs, L. (2000). Climate extremes: Observations, modeling, and impacts. *Science* **289** 2068–2074.
- EASTOE, E. F. and TAWN, J. A. (2009). Modelling non-stationary extremes with application to surface level ozone. *J. R. Stat. Soc. Ser. C. Appl. Stat.* **58** 25–45. [MR2662232](#)
- EDWARDS, P. (2010). *A Vast Machine: Computer Models, Climate Data, and the Politics of Global Warming*. MIT Press, Cambridge, MA.
- HEFFERNAN, J. E. and RESNICK, S. I. (2007). Limit laws for random vectors with an extreme component. *Ann. Appl. Probab.* **17** 537–571. [MR2308335](#)
- HEFFERNAN, J. E. and TAWN, J. A. (2004). A conditional approach for multivariate extreme values. *J. R. Stat. Soc. Ser. B. Stat. Methodol.* **66** 497–546. With discussions and reply by the authors. [MR2088289](#)
- JONATHAN, P. and EWANS, K. (2007). The effect of directionality on extreme wave design criteria. *Ocean Eng.* **34** 1977–1994.
- JONATHAN, P., EWANS, K. and RANDELL, D. (2014). Non-stationary conditional extremes of northern North Sea storm characteristics. *Environmetrics* **25** 172–188. [MR3200308](#)
- KALLACHE, M., VRAC, M., NAVEAU, P. and MICHELANGELI, P.-A. (2011). Nonstationary probabilistic downscaling of extreme precipitation. *J. Geophys. Res.* **116** D05113.
- KEEF, C., PAPANATHOPOULOS, I. and TAWN, J. A. (2013). Estimation of the conditional distribution of a multivariate variable given that one of its components is large: Additional constraints for the Heffernan and Tawn model. *J. Multivariate Anal.* **115** 396–404. [MR3004566](#)
- KINSMAN, B. (2012). *Wind Waves: Their Generation and Propagation on the Ocean Surface*. Dover, New York.
- KYSELÝ, J., PICEK, J. and BERANOVÁ, R. (2010). Estimating extremes in climate change simulations using the peaks-over-threshold method with a non-stationary threshold. *Glob. Planet. Change* **72** 55–68.
- LEDFORD, A. W. and TAWN, J. A. (1996). Statistics for near independence in multivariate extreme values. *Biometrika* **83** 169–187. [MR1399163](#)
- LIU, Y. and TAWN, J. A. (2014). Self-consistent estimation of conditional multivariate extreme value distributions. *J. Multivariate Anal.* **127** 19–35. [MR3188874](#)
- LOFSTED, R. (2014). *Cases in Climate Change Policy: Political Reality in the European Union*. Routledge, London.
- LUGRIN, T., DAVISON, A. C. and TAWN, J. A. (2016). Bayesian uncertainty management in temporal dependence of extremes. *Extremes* **19** 491–515. [MR3535964](#)
- MARAUN, D., WIDMANN, M., GUTIERREZ, J., KOTLARSKI, S., CHANDLER, R., HERTIG, E., WIBIG, J., HUTH, R. and WILCKE, R. (2015). Value: A framework to validate downscaling approaches for climate change studies. *Earth's Future* **3** 1–14.
- MICHELANGELI, P.-A., VRAC, M. and LOUKOS, H. (2009). Probabilistic downscaling approaches: Application to wind cumulative distribution functions. *Geophys. Res. Lett.* **36** 1–6.
- NELSEN, R. B. (2006). *An Introduction to Copulas*, 2nd ed. Springer, New York. [MR2197664](#)
- NORTHROP, P. J. and JONATHAN, P. (2011). Threshold modelling of spatially dependent non-stationary extremes with application to hurricane-induced wave heights. *Environmetrics* **22** 799–809. [MR2861046](#)
- REISTAD, M., BREIVIK, Ø., HAAKENSTAD, H., AARNES, O., FUREVIK, B. and BIDLOT, J. (2011). A high-resolution hindcast of wind and waves for the North Sea, the Norwegian Sea, and the Barents Sea. *J. Geophys. Res.* **116**. C05019.
- ROBINSON, P. M. and TAWN, J. (1997). Statistics for extreme sea currents. *J. R. Stat. Soc. Ser. C. Appl. Stat.* **46** 183–205.
- SILVERMAN, B. W. (1986). *Density Estimation for Statistics and Data Analysis*. Chapman & Hall, London. [MR0848134](#)
- SMITH, R. L. and WEISSMAN, I. (1994). Estimating the extremal index. *J. Roy. Statist. Soc. Ser. B* **56** 515–528. [MR1278224](#)

- SOLOMON, S., QUIN, D., MANNING, M., CHEN, Z., MARQUIS, M., AVERYT, K., TIGNOR, M. and MILLER, H., eds. (2007). *Climate Change 2007—The Physical Science Basis: Working Group I Contribution to the Fourth Assessment Report of the IPCC*. Cambridge Univ. Press, Cambridge.
- TOWE, R. (2015). Modelling the Extreme Wave Climate of the North Sea. Ph.D. thesis, Univ. Lancaster, Lancaster.
- TOWE, R., EASTOE, E., TAWN, J., WU, Y. and JONATHAN, P. (2013). The extremal dependence of storm severity, wind speed and surface level pressure in the northern North Sea. In *ASME 2013 32nd International Conference on Ocean, Offshore and Arctic Engineering*. American Society of Mechanical Engineers, New York.
- VANEM, E., HUSEBY, A. and NATVIG, B. (2012). A Bayesian hierarchical spatio-temporal model for significant wave height in the North Atlantic. *Stoch. Environ. Res. Risk Assess.* **26** 609–632.
- VON MISES, R. (1964). *Mathematical Theory of Probability and Statistics*. Academic Press, New York. [MR0178486](#)
- WADSWORTH, J. L. and TAWN, J. A. (2012). Dependence modelling for spatial extremes. *Biometrika* **99** 253–272. [MR2931252](#)
- WANG, J. and ZHANG, X. (2010). Downscaling and projection of winter extreme daily precipitation over North America. *J. Climate* **21** 923–937.
- WILBY, R., CHARLES, S., ZORITA, E., TIMBAL, B., WHETTON, P. and MEARN, L. (2004). Guidelines for use of climate scenarios developed from statistical downscaling methods. Supporting material of the Intergovernmental Panel on Climate Change.

R. TOWE
SCHOOL OF COMPUTING
AND COMMUNICATIONS
LANCASTER UNIVERSITY
LANCASTER LA1 4WA
UNITED KINGDOM
E-MAIL: r.towe@lancaster.ac.uk

E. EASTOE
J. TAWN
DEPARTMENT OF MATHEMATICS
AND STATISTICS
LANCASTER UNIVERSITY
LANCASTER LA1 4YF
UNITED KINGDOM
E-MAIL: e.eastoe@lancaster.ac.uk
j.tawn@lancaster.ac.uk

P. JONATHAN
STATISTICS AND DATA SCIENCE
SHELL RESEARCH LIMITED
BRABAZON HOUSE
CONCORD BUSINESS PARK
MANCHESTER M22 0RR
UNITED KINGDOM
E-MAIL: philip.jonathan@shell.com